22nd Australasian Fluid Mechanics Conference AFMC2020
Brisbane, Australia, 7–10 December 2020
https://doi.org/10.14264/f0f647c

Linear Stability Analysis of Pulsatile Quasi-Two-Dimensional Duct Flows under a Transverse Magnetic Field

C. J. Camobreco[1], A. Pothérat[2] and G. J. Sheard[1]

[1] Department of Mechanical and Aerospace Engineering, Monash University, VIC 3800, Australia

[2] Fluid and Complex Systems Research Centre, Coventry University, Coventry CV15FB, UK

Abstract

The linear stability of time periodic pulsatile flows under a transverse magnetic field is investigated over a wide range of frequencies. The interplay between variations in frequency and the magnetic field are observed with small amplitude oscillations of the driving force, which can stabilize or destabilize. The complexity rapidly increases with increasing amplitude. High magnetic field strengths are strongly stabilizing, but optimised pulsation amplitudes and frequencies still induce large destabilizations (a 90.3% reduction in critical Reynolds number).

Keywords
Linear Stability; Magnetohydrodynamics; Pulsatile; Duct Flow

Introduction

The transition to turbulence is strongly delayed by the application of a transverse magnetic field to the magnetohydrodynamic (MHD) flow of an electrically conducting fluid. This has implications for the design of self-cooled lead-lithium ducts, which form part of proposed magnetic confinement fusion reactor blankets [8], as the laminar flow transfers insufficient heat from the plasma facing wall [2]. This paper adresses whether a time periodic forcing can advance the critical Reynolds number [7] in MHD flows under strong magnetic fields, as is possible in hydrodynamic flows [11].

The linear stability of pulsatile hydrodynamic channel flows has been assessed in [5, 11], among others. [5, 11] identified the need to validate Floquet methods of stability analysis for pulsatile flows (with time stepping methods) to resolve otherwise dubious or conflicting stability assessments. However, due to these additional numerical costs, the size of the governing three-parameter space and the focus on frequencies related to blood flows, the linear stability picture is far from complete. [5] find that the pulsation frequencies which are (most) destabilizing correspond to those found in blood vessels, with stabilization at much higher and lower frequencies. [11] found that the stabilization or destabilization (depending on frequency) was most intense when the maximum velocity of the pulsatile component is of similar magnitude to that of the steady base flow. However, [5] and [11] do not resolve high Reynolds number conditions. In this work, the additional stabilization due to the imposed magnetic field forces computations to much higher Reynolds numbers (order 10^6 for strong fields); see [6] for the steady problem with a transverse magnetic field.

Magnetoydrodynamic flows, under strong uniform magnetic fields, can become quasi-two-dimensional, such that it is sensible to apply the SM82 model [9]. The magnetic field acts to eliminate velocity gradients along the field lines (by diffusing momentum), to avoid Joule dissipation. This results in a core flow which does not strongly vary along magnetic field lines. Walls perpendicular to the field are instead modelled with linear friction, as the local acceleration within the boundary layer is felt as braking in the core flow.

Problem Description and Methodology

Application is made to a quasi-two-dimensional, time periodic, streamwise (x–direction) flow through a duct of half height L (y–direction), subjected to a uniform magnetic field $B\boldsymbol{e}_z$ directed out-of-plane (z–direction; duct width a), figure 1. The SM82 model is a valid approximation for quasi-two-dimensional flows, such that the governing mass and momentum equations are

$$\boldsymbol{\nabla}_\perp \cdot \boldsymbol{u} = 0, \tag{1}$$

$$Sr\frac{\partial \boldsymbol{u}}{\partial t} = -(\boldsymbol{u}\cdot\boldsymbol{\nabla}_\perp)\boldsymbol{u} - \boldsymbol{\nabla}_\perp p + \frac{1}{Re}\nabla_\perp^2 \boldsymbol{u} - \frac{H}{Re}\boldsymbol{u}, \tag{2}$$

respectively, where time t, velocity $\boldsymbol{u}$, pressure p and the quasi-two-dimensional gradient operator $\boldsymbol{\nabla}_\perp$ have been non-dimensionalized by $1/\omega$, U_1+U_2, $\rho(U_1+U_2)^2$ and L, respectively. ω is the pulsation frequency, U_1 the maximum velocity of the steady base flow component, U_2 the maximum velocity (over one period) of the periodic base flow component, and ρ, ν and σ are the Newtonian fluid's density, kinematic viscosity and electrical conductivity, respectively. There are four non-dimensional parameters, a Reynolds number based on the half duct height $Re = (U_1+U_2)L/\nu$, a Strouhal number $Sr = \omega L/(U_1+U_2)$, a Hartmann friction parameter $H = L^2(2B/a)(\sigma/(\nu\rho))^{1/2}$ and an amplitude ratio $\Gamma = U_1/U_2$. It is also worth defining a Reynolds number ratio $r_s = (Re/(1+1/\Gamma))/Re_{\mathrm{crit,s}}$, where $Re_{\mathrm{crit,s}}$ is the critical Reynolds number for the steady flow ($\Gamma\to\infty$) computed at the same H value.

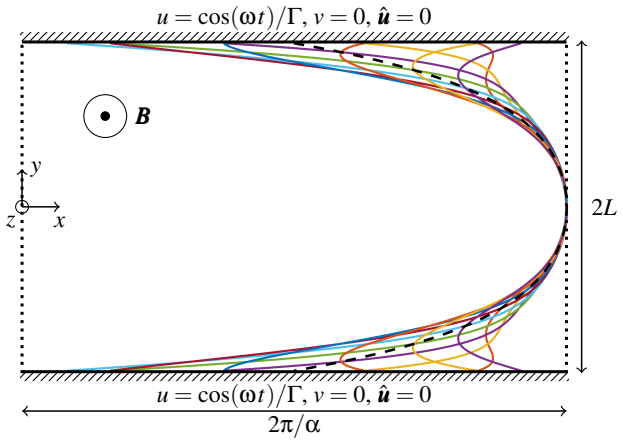

Figure 1. Schematic of the system, with characteristic length of the duct half height L. Solid lines denote oscillating, impermeable and no-slip walls and dotted lines indicate the streamwise extent of the periodic domain, defined by a wave number α. A transverse magnetic field, strength B, is directed into the page. An example of the steady base flow component ($U_{1,\mathrm{B}}$; dashed line) and the normalized total pulsatile base flow ($(1+1/\Gamma)U_{2,\mathrm{B}}$; 11 coloured lines over the full period, 2π) at $H = 10$, $\Gamma = 10$, $Sr = 5\times10^{-3}$ and $Re = 1.5\times10^4$ (close to the conditions optimised for a 90.3% reduction in Re_{crit}) is overlaid.

The quasi-two-dimensional flow approximation is well supported for steady flows [3, 4]. The implications of pulsatility are now considered on two key approximations of the SM82 model: the quasi-static and quasi-two-dimensional approximations [6]. Respectively, in a steady flow, these require that the inertial advection timescale L/U_1 is much larger that the Alfvén time (duct width over Alfvén velocity; to ensure a static field) and the magnetic diffusion time (to ensure two-dimensionality along field lines). The inertial timescale is related to the pulsatile timescale $1/\omega$ through Sr, in the ratio $(L/U_1)/(1/\omega) = Sr(1+1/\Gamma) < 2Sr$ (for $1 < \Gamma < \infty$ considered in this work). Thus if $Sr < 0.5$ (where most of this work is focused) the pulsatile forces act more slowly than inertial forces, and no SM82 approximations are challenged by the periodicity of the driving force. To the author's knowledge, the pulsatile SM82 problem has not been investigated in the literature; there is also very little literature for other magnetic field setups [10].

Considering a fully developed, parallel, time steady flow, driven by a constant pressure gradient such that the maximum velocity is unity, with fixed walls at $y = \pm 1$, the steady base flow component is $U_{1,\mathrm{B}} = (1-\cosh(H^{1/2}y)/\cosh(H^{1/2}))\cosh(H^{1/2})/(\cosh(H^{1/2})-1)$. Considering a time periodic flow $U_{2,\mathrm{B}}(t,y) = U_{2,\mathrm{B}}(t+2\pi,y)$ with walls at $y=\pm1$ oscillating at velocities of $\cos(\omega t)$, taking the Fourier transform of equation (2) provides separable fourth-order equations governing the real and imaginary components of the Fourier coefficients $b(y)$. Once solved for $\Re(b(y))$ and $\Im(b(y))$, taking the inverse Fourier transform yields

$$U_{2,\mathrm{B}} = \Re\left(\frac{\cosh((r+si)y)}{\cosh(r+si)}e^{it}\right) = be^{it} + b^*e^{-it} \qquad (3)$$

where $r = ((SrRe)^2 + H^2)^{1/4}\cos((\tan^{-1}(SrRe/H))/2)$ and $s = ((SrRe)^2+H^2)^{1/4}\sin((\tan^{-1}(SrRe/H))/2)$ are parameters governing the effect of friction on the pulsatile base flow ($r = s = (SrRe/2)^{1/2}$ hydrodynamically), and $*$ represents the complex conjugate. The total base flow is then $U(y,t) = \gamma_1 U_{1,\mathrm{B}} + \gamma_2 U_{2,\mathrm{B}}$ where $\gamma_1 = \Gamma/(1+\Gamma)$ and $\gamma_2 = 1/(1+\Gamma)$ (γ_1 and γ_2 ensure $U_1 + U_2 = 1$).

Instantaneous variables $(\boldsymbol{u}, p)$ are decomposed into base (U,P) and perturbation $(\hat{\boldsymbol{u}},\hat{p})$ components via small parameter ε, as $\boldsymbol{u} = U + \varepsilon\hat{\boldsymbol{u}}$; $p = P + \varepsilon\hat{p}$, to analyse the linear stability with respect to infinitesimal perturbations. After linearising and taking twice the curl of equation (2), substituting equation (1) and assuming plane wave solutions of the form $\hat{v}(y,t) = e^{i\alpha x}\tilde{v}(y,t)$, due to streamwise inhomogeneity, with wave number α, yields

$$\frac{\partial\tilde{v}}{\partial t} = \mathscr{L}^{-1}\left[\frac{i\alpha}{Sr}\frac{\partial^2 U}{\partial y^2} - \frac{U i\alpha}{Sr}\mathscr{L} + \frac{1}{SrRe}\mathscr{L}^2 - \frac{H}{SrRe}\mathscr{L}\right]\tilde{v}, \quad (4)$$

where $\mathscr{L} = (\partial^2/\partial y^2 - \alpha^2)$. The forward evolution of equation (4), from a random initial condition, and with renormalization to unit energy norm at integer period increments, forms the timestepper method of linear stability analysis. Sufficient forward evolution results in all but the fastest growing mode being washed away, and provides the net growth of the leading eigenmode over one period. A Krylov subspace scheme [1] is also implemented to aid convergence and provide the leading few eigenvalues λ_i with largest growth rate. The domain $y \in [-1,1]$ is discretized with N_c+1 Chebyshev nodes. The derivative operators, incorporating boundary conditions, are approximated with spectral derivative matrices [12].

The eigenvalues of the forward evolution operator can also be determined with a Floquet approach [11]. In this case, the time dependence of the perturbation is removed by decomposing into infinite harmonics scaled by exponential growth $\tilde{v}(y,t) = e^{\mu t}\Sigma\tilde{v}_n(y)e^{int}$, with Floquet multiplier μ and harmonic n (numerically truncated to $n \in [-T,T]$). Substituting this decomposition into equation (4) yields a truncated set of coupled ODE's

$$\mu\tilde{v}_n = -\frac{i\alpha}{Sr}M\tilde{v}_{n+1} + \left(\frac{1}{SrRe}\mathscr{L}^{-1}\mathscr{L}^2 - \frac{H}{SrRe} - in - \frac{i\alpha\gamma_1}{Sr}(\mathscr{L}^{-1}(U_{1,\mathrm{B}}\mathscr{L} - \partial^2 U_{1,\mathrm{B}}/\partial y^2))\right)\tilde{v}_n - \frac{i\alpha}{Sr}M^*\tilde{v}_{n-1}, \quad (5)$$

where $M = \gamma_2(\mathscr{L}^{-1}(b\mathscr{L} - \partial^2 b/\partial y^2))$. This system of ODE's is set up as a block tridiagonal system, with the coefficients of $\tilde{v}_{n+1}$, $\tilde{v}_n$ and $\tilde{v}_{n-1}$ placed on super- central- and sub-diagonals, respectively. Spectral derivative matrices are built as before. MATLAB's `eigs` function then finds a subset of eigenvalues of the block tridiagonal system located near zero real component (neutral stability), with convergence tolerance 10^{-14}. For a given Reynolds number, α is then varied until only a single wavenumber, $\alpha_{\max}$, attains zero growth (providing Re_{crit} for specified Sr and Γ).

Results

Variations in r_s (ratio of rescaled pulsatile to steady Re_{crit}) as a function of Sr are depicted for various H at $\Gamma = 100$ (figure 2) and $\Gamma = 10$ (figure 3). Although $\Gamma = 100$ is not very useful for turbulence promotion (the deviation from the steady Re_{crit} values is minimal; between -1% to $+4\%$), it is still sufficient to highlight the underlying mechanics. Hydrodynamically ($H = 10^{-7}$) the steady Re_{crit} is approached ($r_s \to 1$) as $Sr \to 0$ as the oscillation period (2π) is long enough to allow viscosity to smooth out any wall-normal oscillations in the velocity profile over the entire duct (such that no inflection points exist, as in the steady case). As Sr increases, the inflection points are able to be maintained (against the action of viscosity), and the long oscillation period allows for a large amount of intracyclic growth during the deceleration phase of the base flow, thereby reducing Re_{crit}. However, the oscillating boundary layers also become increasingly isolated with increasing Sr, eventually increasing Re_{crit}. With still increasing Sr the oscillation period eventually becomes too small for any relevant intracylcic growth, and the steady result ($r_s \to 1$) is reattained (isolation of the oscillating boundary layers then irrelevant).

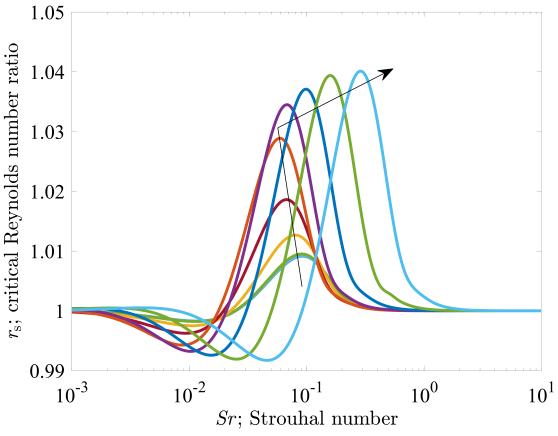

Figure 2. A plot of r_s against Sr at $\Gamma = 100$. Arrow indicates increasing H through 10^{-7}, 0.01, 0.1, 1, 3, 10, 30, 300, 1000.

The effect of the friction parameter is now analysed. For larger friction parameters, as the friction parameter is increased, the curves in figure 2 shift to larger Sr. Increasing H weakens in-

flection points within the pulsatile boundary layer (e.g. a pulsatile isolated SM82 boundary layer has the form $e^{-ry}\cos(sy-t)$, thus increasing H decreases s, thereby eroding wall-normal oscillations in the base flow). Larger Sr values are then required to offset the larger H values, ensuring that inflection points remain within the boundary layer, providing enough intracylic growth to reduce r_s. As such the r_s value of the local minimum does not strongly depend on H. The pulsatile boundary layers also become increasingly separated with increasing H (as r increases), resulting in the steady increase in the r_s value of the local maximum.

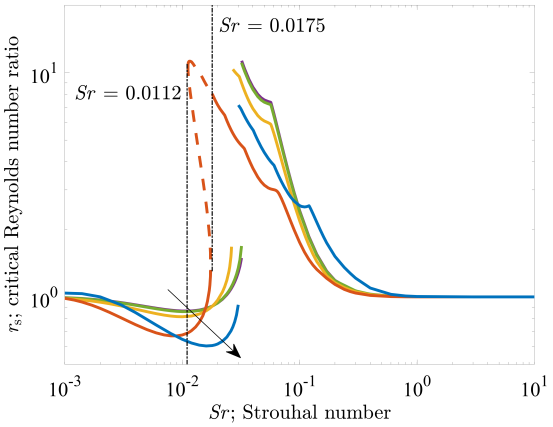

Figure 3. A plot of r_s against Sr at $\Gamma = 10$. Arrow indicates increasing H through 10^{-7}, 0.1, 1, 10, 100. Dashed curves indicate the restabilization, then further destabilization for $Re > Re_{crit}$ at $H = 10$.

The results with a larger amplitude pulsation, $\Gamma = 10$ (figure 3), are now considered. The variation in r_s is now more complicated, although some of the underlying Sr dependence depicted at $\Gamma = 100$ (figure 2) can still be observed. However, a key difference is that the local minima and maxima are more pronounced, due to the greater influence of the pulsatile base flow component. For example, at $H = 10$, a 33.0% reduction or 804% increase over the steady Re_{crit} can be obtained with the appropriate frequency pulsation, with clear benefits for turbulence promotion at $Sr = 9 \times 10^{-3}$. Given the scope of the paper, only a single complexity of the $\Gamma = 10$ behaviour will be investigated, the discontinuous change in r_s, considering $H = 10$.

For a fixed Sr, the maximum growth rate does not always monotonically increase with increasing Re. As such, a dashed curve is plotted on figure 3 as a function of Sr for the $H = 10$, $\Gamma = 10$ case considered, indicating a region of restabilization (with the stable region under the now continuous solid-dashed-solid curve). At $Sr = 0.017$ (the discontinuity is at $Sr \approx 0.0175$), depicted for a wide range of Re in figure 4, the initial destabilization occurs at $Re_{crit} = 8.50617 \times 10^4$. The maximum growth rate increases with increasing Re until $Re \approx 1.1 \times 10^5$. Further increasing Re (which further isolates the boundary layers at fixed Sr) induces stabilization, with only negative growth (stability) reattained at $Re = 1.52788 \times 10^5$. With still increasing Re the single eigenmode almost completely vanishes. Finally, with still further increases in Re, multiple similar modes (eventually four are visible in figure 4) are excited, one of which first attains positive growth at $Re = 6.70474 \times 10^5$. It is a similar story at $Sr = 0.018$, figure 5, with one key exception. The single eigenmode which is visible at lower Re is not able to attain positive growth rates, before it eventually becomes subdominant. As such neutral stability is first encountered at the substantially higher $Re_{crit} = 6.40840 \times 10^5$, explaining the discontinuity in the r_s curves at $\Gamma = 10$ (figure 3). The stable regions can be further clarified by considering the neutral (zero growth) curves, figure 6. There is no unstable region at lower Re when $Sr = 0.018$. At $Sr < 0.0175$ a closed unstable region appears, which rapidly occupies more of the wave number space with decreasing Sr. Eventually the closed curves intersect the open curves (for $Sr < 0.0112$), such that their is no longer a restabilization region if increasing Re at fixed Sr.

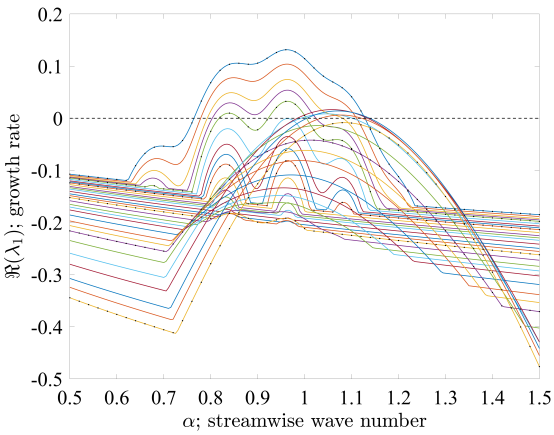

Figure 4. Exponential growth rate as a function of α with increasing Re (8×10^4 through 8×10^5) at $Sr = 0.017$. Destabilization first occurs at $Re_{crit} = 8.50617 \times 10^4$, with restabilzation at $Re = 1.52788 \times 10^5$ and then a final destabilization at $Re = 6.70474 \times 10^5$. Symbols (timestepper) show excellent agreement with curves (Floquet).

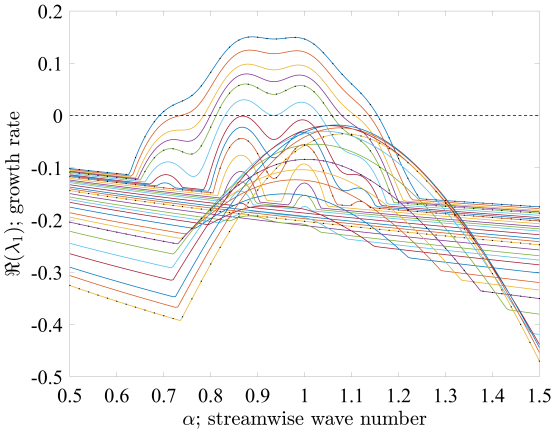

Figure 5. Exponential growth rate as a function of α with increasing Re (8×10^4 through 8×10^5) at $Sr = 0.018$. The single peak mode does not attain positive growth rates at this Sr, thus $Re_{crit} = 6.40840 \times 10^5$ is much larger than Re_{crit} when $Sr = 0.017$. Symbols (timestepper) show excellent agreement with curves (Floquet).

The local minima in r_s occur at Sr values which should be unstable for all $Re > Re_{crit}$. As such, variations over the $1 < \Gamma < 100$ and $10^{-3} < Sr < 1$ space were performed to determine the greatest advancement in Re_{crit}. Recall for $H = 10$, the $\approx 33\%$ reduction in Re_{crit} relative to the steady value at $\Gamma = 10$. The local minimum at $H = 10$ was located at $\Gamma = 1.19$, $Sr = 5.3 \times 10^{-3}$, with $r_s = 0.0973$, a 90.3% reduction from the steady critical Reynolds number, which is very promising for the application of turbulence promotion. As discussed for $\Gamma = 100$, the local minimum is less sensitive to H, and thus it is likely that a large reduction in the critical Reynolds number

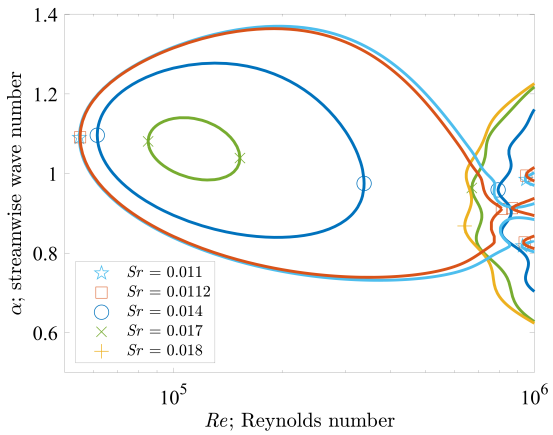

Figure 6. Neutral (zero growth rate) curves for various Sr, at $\Gamma = 10$, $H = 10$. Unstable (positive growth) regions are inside the closed curves, and to the right of the open curves.

could be attained with the appropriate frequency and amplitude pulsation at even fusion relevant magnetic field strengths.

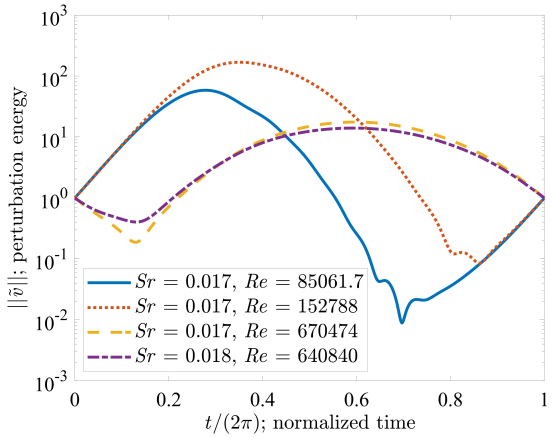

Figure 7. Intracylcic growth at the four critical (no net growth) conditions at $Sr = 0.017$ (destabilization, restabilization, and then destabilization again) and $Sr = 0.018$ (initial destabilization), at $\Gamma = 10$, $H = 10$.

As a final note, the intracyclic growth is displayed for the $Sr = 0.017$ and $Sr = 0.018$ cases discussed earlier. The larger intracyclic growth at lower Reynolds numbers bodes well for the possibility for bypass transitions (even without optimised perturbations) via large amounts of transient growth. This should further advance the Reynolds number which incites transition.

Conclusions

The linear stability of time periodic flows was investigated over a wide range of frequencies and magnetic field strengths. A maximum destabilization was optimised over all frequencies, and all amplitude ratios greater than unity, demonstrating potential for a 90.3% reduction in critical Reynolds number at moderate field strength. This bodes well for the introduction of turbulence in lead-lithium coolant duct flows, as, although they are subjected to much larger magnetic field strengths, the destabilization (percentage) slightly improves with increasing field strength. Furthermore, large amounts of intracylcic growth were observed, which may allow subcritical bypass transition scenarios, and which is an avenue for future work.

Acknowledgements

C.J.C. receives an Australian Government Research Training Program (RTP) Scholarship. A.P. is supported by Wolfson Research Merit Award Scheme grant WM140032 from the Royal Society. This research was supported by the Australian Government via the Australian Research Council (Discovery Grants DP150102920 and DP180102647), the National Computational Infrastructure (NCI) and Pawsey Supercomputing Centre (PSC), and, in particular, Monash University via the MonARCH HPC cluster.

References

[1] Barkley, D., Blackburn, H. M., and Sherwin, S. J. (2008). Direct optimal growth analysis for timesteppers. *Int. J. Numer. Methods Fluids*, 57, 1435–1458 (DOI: 10.1002/fld.1824).

[2] Cassels, O. G. W., Hussam, W. K., and Sheard, G. J. (2016). Heat transfer enhancement using rectangular vortex promoters in confined quasi-two-dimensional magnetohydrodynamic flows. *Int. J. Heat Mass Transf.*, 93, 186–199 (DOI: 10.1016/j.ijheatmasstransfer.2015.10.006).

[3] Cassels, O. G. W., Vo, T., Pothérat, A., and Sheard, G. J. (2018). From three-dimensional to quasi-two-dimensional: transient growth in magnetohydrodynamic duct flows. *J. Fluid Mech.*, 861, 382–406 (DOI: 10.1017/jfm.2018.863).

[4] Kanaris, N., Albets X., Grigoriadis, D., and Kassinos, S. (2013). Three-dimensional numerical simulations of magnetohydrodynamic flow around a confined circular cylinder under low, moderate, and strong magnetic fields. *Phys. Fluids*, 25(7), 074102 (DOI: 10.1063/1.4811398).

[5] Pier, B., and Schmid, P. J. (2017). Linear and nonlinear dynamics of pulsatile channel flow. *J. Fluid Mech.*, 815, 435–480 (DOI: 10.1017/jfm.2017.58)

[6] Pothérat, A. (2007). Quasi-two-dimensional perturbations in duct flows under transverse magnetic field. *Phys. Fluids*, 19(7), 074104 (DOI: 10.1063/1.2747233).

[7] Schmid, P. J., and Henningson, D. S. (2001). *Stability and Transition in Shear Flows*. Springer-Verlag New York (DOI: 10.1007/978-1-4613-0185-1).

[8] Smolentsev, S., Moreau, R., and Abdou, M. (2008). Characterization of key magnetohydrodynamic phenomena in PbLi flows for the US DCLL blanket. *Fusion Eng. Des.*, 83(5), 771–783 (DOI: 10.1016/j.fusengdes.2008.07.023).

[9] Sommeria, J. and Moreau, R. (1982). Why, how, and when, MHD turbulence becomes two-dimensional. *J. Fluid Mech.*, 118, 507–518 (DOI: 10.1017/S0022112082001177).

[10] Thomas, C., Bassom, A. P., and Davies, C. (2010). The linear stability of a Stokes layer with an imposed axial magnetic field. *J. Fluid Mech.*, 662, 320–328 (DOI: 10.1017/S0022112010004210).

[11] Thomas, C., Bassom, A. P., Blennerhassett, P. J., and Davies, C. (2011). The linear stability of oscillatory Poiseuille flow in channels and pipes. *Proc. R. Soc. A*, 467, 2643–2662 (DOI: 10.1098/rspa.2010.0468).

[12] Trefethen, L. N. (2000). *Spectral Methods in MATLAB*. Society for Industrial and Applied Mathematics (DOI: 10.1137/1.9780898719598).